Bonding analysis in ytterbium(II) distannyl and related tetryls

Peter M Chapple, Julien Cartron, Ghanem Hamdoun, Marie Cordier, Samia Kahlal, Hassan Oulyadi, Jean-François Carpentier, Jean-Yves Saillard, Yann Sarazin

Bonding analysis in ytterbium(II) distannyl and related tetryls

Peter M. Chapple,[a] Julien Cartron,[a] Ghanem Hamdoun,[b] Marie Cordier,[a] Samia Kahlal,[a] Hassan Oulyadi,[c] Jean-François Carpentier,[a] Jean-Yves Saillard*[a] and Yann Sarazin*[a]

[a] Univ Rennes, CNRS, ISCR-UMR 6226, 35000 Rennes (France). E-mail : yann.sarazin@univ-rennes1.fr

[b] Euromed University of Fes (UEMF), Fez, Morocco

[c] Normandie Université, Laboratoire COBRA (UMR 6014 & FR 3038), 76000 Rouen (France).

Corresponding authors: yann.sarazin@univ-rennes1.fr
jean-yves.saillard@univ-rennes1.fr

ORCID

JF. Carpentier	0000-0002-9160-7662
P. M. Chapple	0000-0003-0402-6948
M. Cordier	0000-0003-0917-2725
H. Oulyadi	0000-0001-5813-1482
JY. Saillard	0000-0003-4469-7922
Y. Sarazin	0000-0003-1121-0292

† Electronic Supplementary Information (ESI) available: detailed synthetic procedures, spectroscopic data, XRD diffraction analysis for **Yb-Sn** and **Yb-Ge** (CCDC 2060120-2060121) and details of DFT calculations. See DOI: 10.1039/x0xx00000x

Abstract

The syntheses of the ytterbium(II) distannyl [Yb{Sn(SiMe$_3$)$_3$}$_2$.(thf)$_4$] (**Yb-Sn**) and of its digermyl analogue [Yb{Ge(SiMe$_3$)$_3$}$_2$.(thf)$_3$] (**Yb-Ge**) are presented. The compounds were characterised by multinuclear high-resolution solution NMR spectroscopy, including ^{171}Yb NMR, and by X-ray diffraction crystallography. The bonding and electronic properties of the two complexes, along with those of the known ytterbium(II) disilyl derivative [Yb{Si(SiMe$_3$)$_3$}$_2$.(thf)$_3$] (**Yb-Si**) and those of the congeneric calcium distannyl [Ca{Sn(SiMe$_3$)$_3$}$_2$.(thf)$_4$] (**Ca-Sn**), were investigated in detail by DFT calculations. This analysis points at a primarily ionic Yb-tetrel bonding, with a small covalent contribution, attributed principally to the 5*d*(Yb) participation. This weak covalent character is found to be larger for the distannyl **Yb-Sn** than for its lighter Si- and Ge-derivatives. The covalent component is also found to be greater in **Yb-Sn** than in **Ca-Sn**, due to the availability of the 5*d*(Yb) orbitals for bonding.

Introduction

Salts and soluble complexes of the classical divalent lanthanides ytterbium, europium and samarium have long attracted interest as one-electron reducing agents, for the activation of small molecules[1-6] and, more recently, for their magnetic properties[7-8] or as potent catalysts.[9-15] Compared to its congeners, the smallest of these elements, Yb(II), offers the advantage of being diamagnetic due to its closed-shell [Xe] $4f^{14}$ $6s^2$ electronic configuration. The ^{171}Yb isotope, with a spin number of ½, a natural abundancy of 14.31% and a reasonable receptivity (4.4 vs carbon), is a nucleus well suited to NMR spectroscopy. ^{171}Yb chemical shifts measured so far are in the range +2500 to –500 ppm. ^{171}Yb NMR spectroscopy has provided useful information on the structural and bonding parameters in a variety of ytterbium(II) complexes[16] since this spectroscopic method was first used on a range of amido and cyclopentadienyl species.[17]

We have recently prepared two series of alkaline-earth distannyls [Ae(SnR$_3$)$_2$.(thf)$_x$], for Ae = Ca, Sr and Ba and where R = Ph or SiMe$_3$.[18] We have also reported heteroleptic Ae-stannyls and Ae-silyl [{L}AeE(SiMe$_3$)$_2$.(thf)$_x$] for Ae = Ca and Ba and E = Si or Sn, and where L is a sterically demanding, tridentate bis(imino)carbabazolate.[19-20] Ytterbium(II) is often compared to calcium due to their similar physico-chemical properties, notably their ionic radii (Ca^{2+}: 1.00 Å; Yb^{2+}: 1.02 Å), Pauling electronegativity (Ca, 1.00; Yb, 1.1) and oxophilicity. We have hence turned our attention to the synthesis of ytterbium(II) tetryls, on the grounds that the characterisation and structural analysis of complete homologous suites of such complexes have not been performed to date. The first ytterbium(II) stannyl, the tetrahedral [Yb{Sn(CH$_2$^{t}Bu)$_3$}$_2$.(thf)$_2$], was reported and crystallographically characterised in 1991;[21] multinuclear NMR data recorded in toluene-d_8 showed diagnostic resonances at δ ^{171}Yb 725 ppm and δ ^{119}Sn –95 ppm in the ^{171}Yb and ^{119}Sn NMR spectra. Bochkarev and coworkers described the molecular solid-state structures of the octahedral [Yb(SnPh$_3$)$_2$.(thf)$_4$][22] and [Yb{Sn(SnMe$_3$)$_3$}$_2$.(thf)$_4$],[23] and that of the heteroleptic [(thf)$_2$.(Ph$_3$Sn)Yb(μ-Ph)$_3$Yb.(thf)$_3$],[24] but ^{171}Yb NMR data was not provided. The same group also disclosed the only two structurally identified ytterbium(II) germyls known to date, [Yb(GePh$_3$)$_2$.(thf)$_4$] and the metallacycle [*cyclo*-(Ph$_2$Ge)$_4$Yb.(thf)$_4$], where the geometry about the Yb(II) atoms is octahedral.[25-26] They also mentioned the first structurally characterised ytterbium(II)-silyl, [Yb(SiPh$_3$)$_2$.(thf)$_4$], said to be isostructural with the germyl congener,[26] but the X-ray structure was not provided and is currently not available.[27] Baumgartner and coworkers demonstrated the detailed syntheses and structures of the hypersilylated trisolvate [Yb{Si(SiMe$_3$)$_3$}$_2$.(thf)$_3$], which adopts a distorted trigonal pyramidal geometry, and those of the metallacycle [{Me$_2$Si(Me$_3$Si)$_2$Si}$_2$Yb.(thf)$_4$];[28] unfortunately, the ^{171}Yb NMR data was not given, although $^1J_{^{29}Si\text{-}^{171}Yb}$ and $^2J_{^{29}Si\text{-}^{171}Yb}$ scalar coupling were visible in the ^{29}Si NMR spectra for these complexes. Over ten other X-ray structures of Yb(II)-silyls are available in the CCDC database, e.g. the seminal [(C$_5$Me$_5$)Yb{Si(SiMe$_3$)$_3$}.(thf)$_2$] (δ ^{171}Yb 421 ppm and $|^1J_{^{171}Yb\text{-}^{29}Si}|$ = 829 Hz in toluene-d_8),[29] and the three-coordinate [KYb{Si(SiMe$_3$)$_3$}{N(SiMe$_3$)$_2$}$_2$] (δ ^{171}Yb 1057 ppm, $|^1J_{^{171}Yb\text{-}^{29}Si}|$ = 716 Hz, $|^2J_{^{171}Yb\text{-}^{29}Si}|$ = 5.0-8.9 Hz;

solvent benzene-d_6).[30] Finally, the organoytterbium(II) [Yb{C(SiMe$_3$)$_3$}$_2$], which exhibits a very bent geometry (C-Sn-C' = 104.8(5)°) with secondary Yb···H$_3$C interactions in the molecular solid-state, has long been known;[31] it displays a resonance at 812 ppm in the ^{171}Yb NMR spectrum recorded in toluene-d_8. Ytterbium(II) plumbyls are unknown to date. All relevant existing complexes were surveyed in a recent review.[32]

We report here on the synthesis, structural determination and multi-nuclear high-resolution NMR characterisation of two new ytterbium(II) tetryls, [Yb{Ge(SiMe$_3$)$_3$}$_2$.(thf)$_3$] (**Yb-Ge**) and its heavier analogue [Yb{Sn(SiMe$_3$)$_3$}$_2$.(thf)$_4$] (**Yb-Sn**). Their structural and electronic parameters, as well as those of the known silyl derivative [Yb{Si(SiMe$_3$)$_3$}$_2$.(thf)$_3$] (**Yb-Si**),[28] have been analysed by the means of DFT calculations to inform ourselves about the bonding properties in this family of complexes (Figure 1). The results of this analysis, along with a comparison of the bonding patterns between **Yb-Sn** and its calcium congener [Ca{Sn(SiMe$_3$)$_3$}$_2$.(thf)$_4$] (**Ca-Sn**),[18] are described herein.

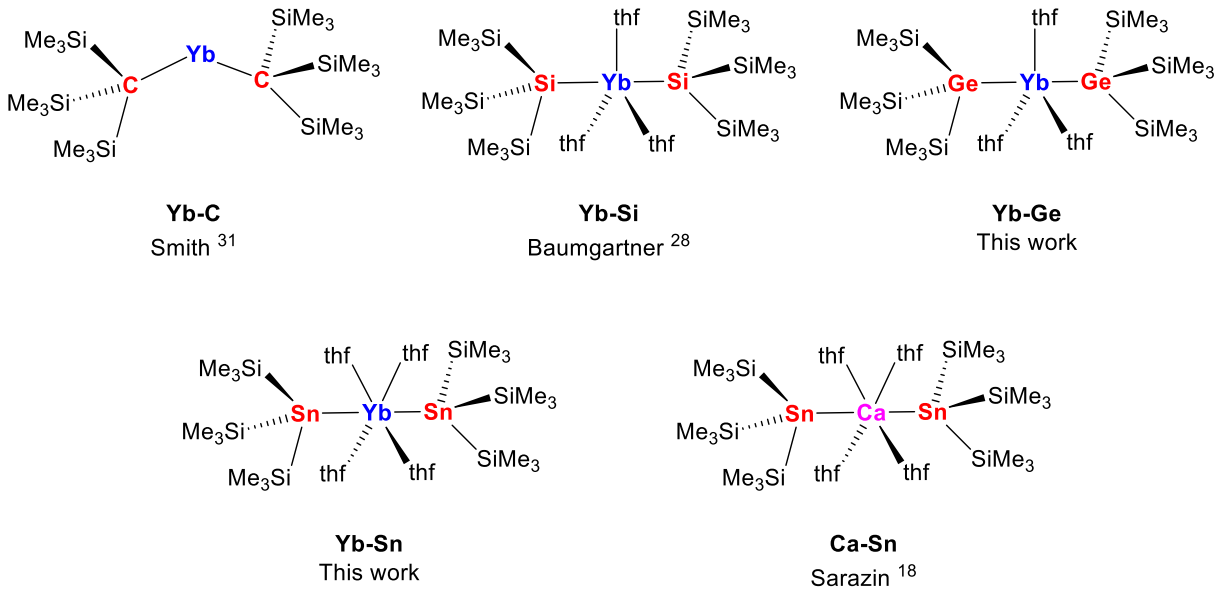

Figure 1. Ytterbium(II) tetryls (**Yb-Si**, **Yb-Ge** and **Yb-Sn**) investigated here, and their known **Yb-C** hydrocarbyl and **Ca-Sn** derivatives.

Results and Discussion

Synthesis and characterisation

Large crops of crystals of the complexes [Yb{Ge(SiMe$_3$)$_3$}$_2$.(thf)$_3$] (**Yb-Ge**, dark yellow/orange crystals) and [Yb{Sn(SiMe$_3$)$_3$}$_2$.(thf)$_4$] (**Yb-Sn**, pale yellow crystals) were isolated in non-optimised 31-42% yields following the stoichiometric reactions in thf between YbI$_2$.(thf)$_2$ and *in-situ* generated [K{E(SiMe$_3$)$_3$}.(thf)$_x$] (E = Ge, Sn;[33-34] Scheme 1). The complexes were characterised by XRD and high-resolution multinuclear NMR spectroscopy, including ^{171}Yb NMR. The compounds dissolve well in all common organic solvents, including aliphatic hydrocarbons. The coordinated thf molecules cannot be removed by drying under dynamic vacuum.

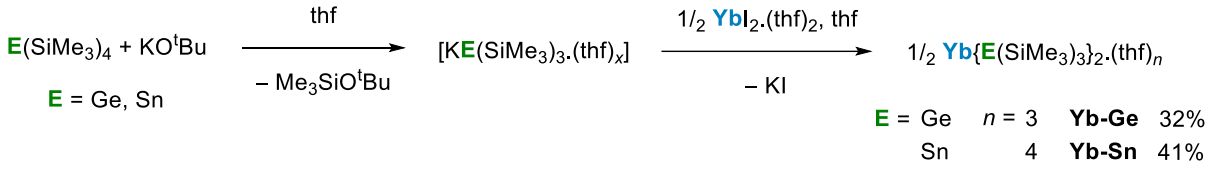

Scheme 1. One-pot synthesis of [Yb{Ge(SiMe$_3$)$_3$}$_2$.(thf)$_3$] (**Yb-Ge**) and [Yb{Ge(SiMe$_3$)$_3$}$_2$.(thf)$_4$] (**Yb-Sn**).

The ^{1}H NMR spectrum for the distannyl **Yb-Sn** collected in benzene-d_6 features three somewhat broad resonances for the coordinated thf molecules ($\delta_{^1H}$ 3.80 and 1.47ppm) and for the Si*Me*$_3$ moiety (0.57 ppm). The ^{29}Si{^{1}H} NMR spectrum (Figure 2) is characterised by a singlet at $\delta_{^{29}Si}$ –10.9 ppm, with observable coupling to Sn ($|^1J_{^{29}Si\text{-}^{119}Sn}|$ = 66.2 Hz, $|^1J_{^{29}Si\text{-}^{117}Sn}|$ = 63.1 Hz, $|^3J_{^{29}Si\text{-}^{117/119}Sn}|$ = 5.4 Hz), Yb ($|^2J_{^{29}Si\text{-}^{171}Yb}|$ = 30.5 Hz), and C ($|^1J_{^{29}Si\text{-}^{13}C}|$ = 37.5 Hz). The ^{119}Sn{^{1}H} NMR spectrum (Figure 3) also displays a singlet resonance at $\delta_{^{119}Sn}$ –757 ppm with observable $^1J_{^{119}Sn\text{-}^{171}Yb}$ coupling to ^{171}Yb and $^2J_{^{119}Sn\text{-}^{117}Sn}$ coupling to Sn ($|^1J_{^{119}Sn\text{-}^{171}Yb}|$ = 5570 Hz and $|^2J_{^{119}Sn\text{-}^{117}Sn}|$ = 932 Hz). Relative integrals were used to help assign couplings in particularly crowded spectra, such as in Figure 2. The ^{171}Yb NMR spectrum (Figure 4) shows a broad singlet at $\delta_{^{171}Yb}$ 535 ppm ($\Delta\nu_{1/2}$ = 360 Hz) and the $^1J_{^{171}Yb\text{-}^{117/119}Sn}$ couplings can be observed but not fully resolved for the ^{119}Sn/^{117}Sn isotopes; hence, the coupling constant given in Table 1 is the value determined from the ^{119}Sn NMR data.

Compound **Yb-Ge** gives rise to similar resonances in its ^{1}H NMR spectrum for thf ($\delta_{^1H}$ 3.69 and 1.41 ppm) and for Si*Me*$_3$ (0.53 ppm), but they are high-field shifted compared to **Yb-Sn**. The single resonance in the ^{29}Si{^{1}H} DEPT NMR spectrum of **Yb-Ge** at $\delta_{^{29}Si}$ –2.4 ppm is shifted downfield relative to **Yb-Sn,** and is more in line with the chemical shift reported for the similar compound [Yb{Si(*Si*Me$_3$)$_3$}$_2$.(thf)$_3$] (**Yb-Si**, $\delta_{^{29}Si}$ –5.2 ppm).[28] The large variation in the chemical shift compared to **Yb-Sn** is most likely due to the change in the coordination environment about the central metal from a 6-coordinate to a 5-coordinate complex, while the different nature of the bonding may also be invoked (see DFT discussion below) as a possible contribution. Electronic factors depending on the nature of the anion for E = Si, Ge or Sn may also be partly responsible for the observed variation of chemical shifts.

The $|^2J_{^{29}Si\text{-}^{171}Yb}|$ coupling constant of 20.2 Hz for **Yb-Ge** is significantly smaller than that in **Yb-Sn** (30.5 Hz). The ^{171}Yb NMR displays a slightly broad singlet at $\delta_{^{171}Yb}$ 816 ppm ($\Delta\nu_{1/2}$ = 160 Hz), shifted downfield from that of **Yb-Sn**.

Although the complex **Yb-Si** has already been reported,[28] its ^{171}Yb NMR spectrum was not included in its characterisation. Hence, we remade this complex in order to gather its full suite of NMR spectra, and to make comparisons with **Yb-Sn** and **Yb-Ge**. Complex **Yb-Si** was prepared as described, though the NMR data we recorded does have a few subtle differences from the literature data, most importantly the difference in the $|^2J_{^{29}Si\text{-}^{171}Yb}|$ coupling constant of 8.6 Hz (reported previously to be 41 Hz, a constant that we propose is actually from $|^1J_{^{29}Si\text{-}^{13}C}|$ scalar coupling).[28] The ^{171}Yb NMR spectrum of **Yb-Si** has a broad resonance similar to that of **Yb-Ge**. This signal ($\delta_{^{171}Yb}$ 948 ppm) is shifted downfield relative to **Yb-Sn** ($\delta_{^{171}Yb}$ 535 ppm) and **Yb-Ge** ($\delta_{^{171}Yb}$ 816 ppm). Hence, the resonance becomes more deshielded for the lighter tetrels in group 14. For comparison, the resonance in the NMR spectrum of the unsolvated [Yb{C(SiMe$_3$)$_3$}$_2$] was found at $\delta_{^{171}Yb}$ 812 ppm.[31] However, direct comparison between the compounds is ill-advised due to their different degree of solvation by thf molecules.

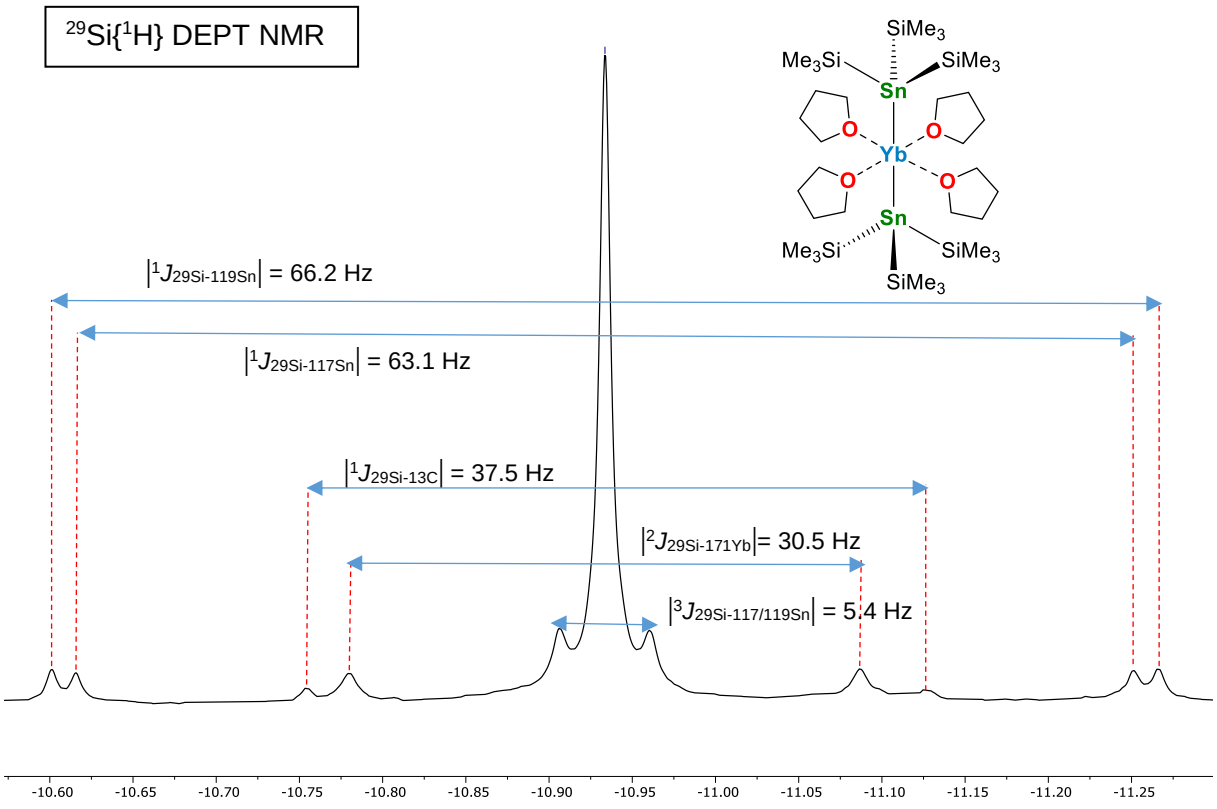

Figure 2. ^{29}Si{^{1}H} DEPT NMR spectrum (99.36 MHz, benzene-d_6, 300 K) of [Yb{Sn(SiMe$_3$)$_3$}$_2$.(thf)$_4$] (**Yb-Sn**).

A summary of the NMR data for compounds **Yb-Si**, **Yb-Ge** and **Yb-Sn** is collated in Table 1. The data for $[Ca\{Sn(SiMe_3)_3\}_2.(thf)_4]$ (**Ca-Sn**), that is, the direct calcium analogue of **Yb-Sn** recently prepared, has also been added. Compared to **Ca-Sn**, the ^{119}Sn resonance for **Yb-Sn** is slightly deshielded (–857 vs –757 ppm, respectively) whereas remarkably, the absolute value of $^2J_{^{119}Sn\text{-}^{117}Sn}$ for the scalar coupling of the tin isotopes through the central metal is more than doubled (455 and 932 Hz, respectively). This is presumed to reflect the presence of the $4f^{14}$ electrons and the slightly more covalent bonding in **Yb-Sn**, although we will refrain from making further claims at this stage. We note that the potassium stannylide $[KSn(SiMe_3)_3]$, either as a 18-c-6 crown ether adduct in benzene-d_6 ($\delta_{^{119}Sn}$ –892.2 ppm, $\delta_{^{29}Si}$ –12.7 ppm, $|^1J_{^{29}Si\text{-}^{119}Sn}| = 271$ Hz, $|^1J_{^{29}Si\text{-}^{117}Sn}| = 259$ Hz) or as a solution in dimethoxyethane ($\delta_{^{119}Sn}$ –896.8 ppm, $\delta_{^{29}Si}$ –12.9 ppm, $|^1J_{^{29}Si\text{-}^{119}Sn}| = 295$ Hz, $|^1J_{^{29}Si\text{-}^{117}Sn}| = 282$ Hz) display chemical shifts that are very similar to those of **Yb-Sn** and **Ca-Sn**, although the tin-to-silicon coupling constants are much larger for the alkali salt.[33]

Table 1. Summary of NMR spectroscopic data for complexes [Met{E(SiMe$_3$)$_3$}$_2$.(thf)$_n$] (Met = Yb: E = Sn, *n* = 4, **Yb-Sn**; Ge, *n* = 3, **Yb-Ge**; Si, *n* = 3, **Yb-Si**; Met = Ca, E = Sn, *n* = 4, **Ca-Sn**).[a]

	^{171}Yb NMR		^{119}Sn{^{1}H} NMR		^{29}Si{^{1}H} NMR		^{13}C{^{1}H} NMR	
	δ ^{171}Yb / [ppm]	$\lvert^nJ_{X\text{-}Y}\rvert$ / [Hz]	δ ^{119}Sn / [ppm]	$\lvert^nJ_{X\text{-}Y}\rvert$ / [Hz]	δ ^{29}Si / [ppm]	$\lvert^nJ_{X\text{-}Y}\rvert$ / [Hz]	δ ^{13}C [ppm]	$\lvert^nJ_{X\text{-}Y}\rvert$ / [Hz]
[Yb{Sn(SiMe$_3$)$_3$}$_2$.(thf)$_4$] (**Yb-Sn**)	535	$\lvert^1J_{^{171}Yb\text{-}^{119}Sn}\rvert$ = 5570	–757	$\lvert^1J_{^{119}Sn\text{-}^{171}Yb}\rvert$ = 5570 $\lvert^2J_{^{119}Sn\text{-}^{117}Sn}\rvert$ = 932	*Si*Me$_3$ = –10.9	$\lvert^1J_{^{29}Si\text{-}^{119}Sn}\rvert$ = 66.2 $\lvert^1J_{^{29}Si\text{-}^{117}Sn}\rvert$ = 63.1 $\lvert^1J_{^{29}Si\text{-}^{13}C}\rvert$ = 37.5 $\lvert^2J_{^{29}Si\text{-}^{171}Yb}\rvert$ = 30.5 $\lvert^3J_{^{29}Si\text{-}^{117/119}Sn}\rvert$ = 5.4	6.75	$\lvert^1J_{^{13}C\text{-}^{29}Si}\rvert$ = 37.5 $\lvert^2J_{^{13}C\text{-}^{117/119}Sn}\rvert$ = 6.7
[Yb{Ge(SiMe$_3$)$_3$}$_2$.(thf)$_3$] (**Yb-Ge**)	816	not detected	n/a	n/a	*Si*Me$_3$ = –2.4	$\lvert^1J_{^{29}Si\text{-}^{13}C}\rvert$ = 37.5 $\lvert^2J_{^{29}Si\text{-}^{171}Yb}\rvert$ = 20.2	7.32	$\lvert^1J_{^{13}C\text{-}^{29}Si}\rvert$ = 37.5 $\lvert^3J_{^{13}C\text{-}^{171}Yb}\rvert$ = 6.8
[Yb{Si(SiMe$_3$)$_3$}$_2$.(thf)$_3$] (**Yb-Si**)[28]	948	not detected	n/a	n/a	*Si*Me$_3$ = –5.2 *Si*Si = −145.9	$\lvert^1J_{^{29}Si\text{-}^{13}C}\rvert$ = 38.8 ±2.1[c] $\lvert^1J_{^{29}Si\text{-}^{29}Si}\rvert$ = 28.2 $\lvert^2J_{^{29}Si\text{-}^{171}Yb}\rvert$ = 8.6 $\lvert^1J_{^{29}Si\text{-}^{171}Yb}\rvert$ = 728 $\lvert^1J_{^{29}Si\text{-}^{29}Si}\rvert$ = 28.2	7.89	$\lvert^1J_{^{13}C\text{-}^{29}Si}\rvert$ = 38.8 ±2.1[b] $\lvert^2J_{^{13}C\text{-}^{29}Si}\rvert$ = 4.8 $\lvert^3J_{^{13}C\text{-}^{171}Yb}\rvert$ = 20.8
[Ca{Sn(SiMe$_3$)$_3$}$_2$.(thf)$_4$] (C**a-Sn**)[18]	n/a	n/a	–857	$\lvert^1J_{^{119}Sn\text{-}^{29}Si}\rvert$ = 82.1 $\lvert^2J_{^{119}Sn\text{-}^{117}Sn}\rvert$ = 455	*Si*Me$_3$ = –12.9	$\lvert^1J_{^{29}Si\text{-}^{119}Sn}\rvert$ = 82.9 $\lvert^1J_{^{29}Si\text{-}^{117}Sn}\rvert$ = 79.0 $\lvert^1J_{^{29}Si\text{-}^{13}C}\rvert$ = 36.7 $\lvert^3J_{^{29}Si\text{-}^{117/119}Sn}\rvert$ = 2.7	7.76	$\lvert^1J_{^{13}C\text{-}^{29}Si}\rvert$ = 36.7 $\lvert^2J_{^{13}C\text{-}^{117/119}Sn}\rvert$ = 19.3

[a] NMR data recorded in benzene-d_6 from crystalline samples. Chemical shifts given in ppm and coupling constants in Hz. [b] The exact values of $\lvert^1J_{^{13}C\text{-}^{29}Si}\rvert$ determined by ^{29}Si{^{1}H} and ^{13}C{^{1}H} were, respectively, 40.9 and 36.7 Hz.

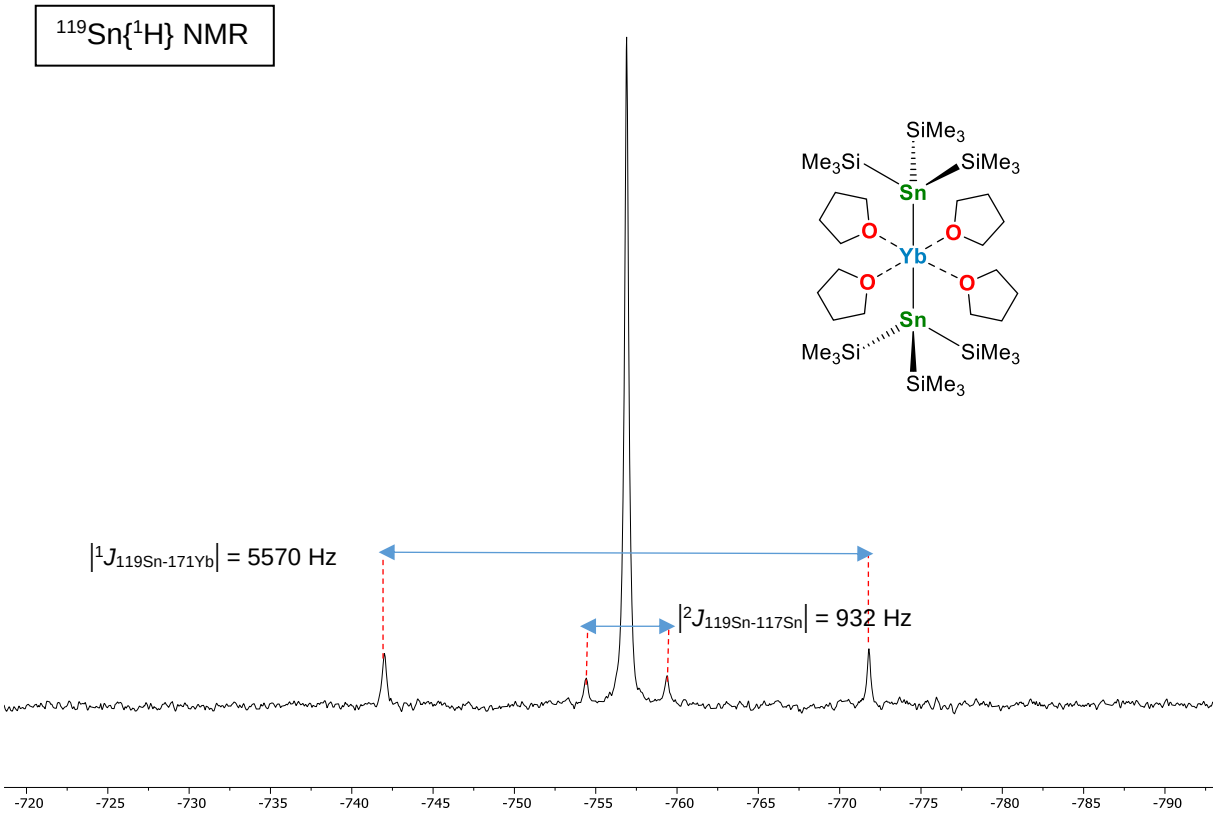

Figure 3. ^{119}Sn{^{1}H} NMR spectrum (186.36 MHz, benzene-d_6, 300 K) of [Yb{Sn(SiMe$_3$)$_3$}$_2$.(thf)$_4$] (**Yb-Sn**).

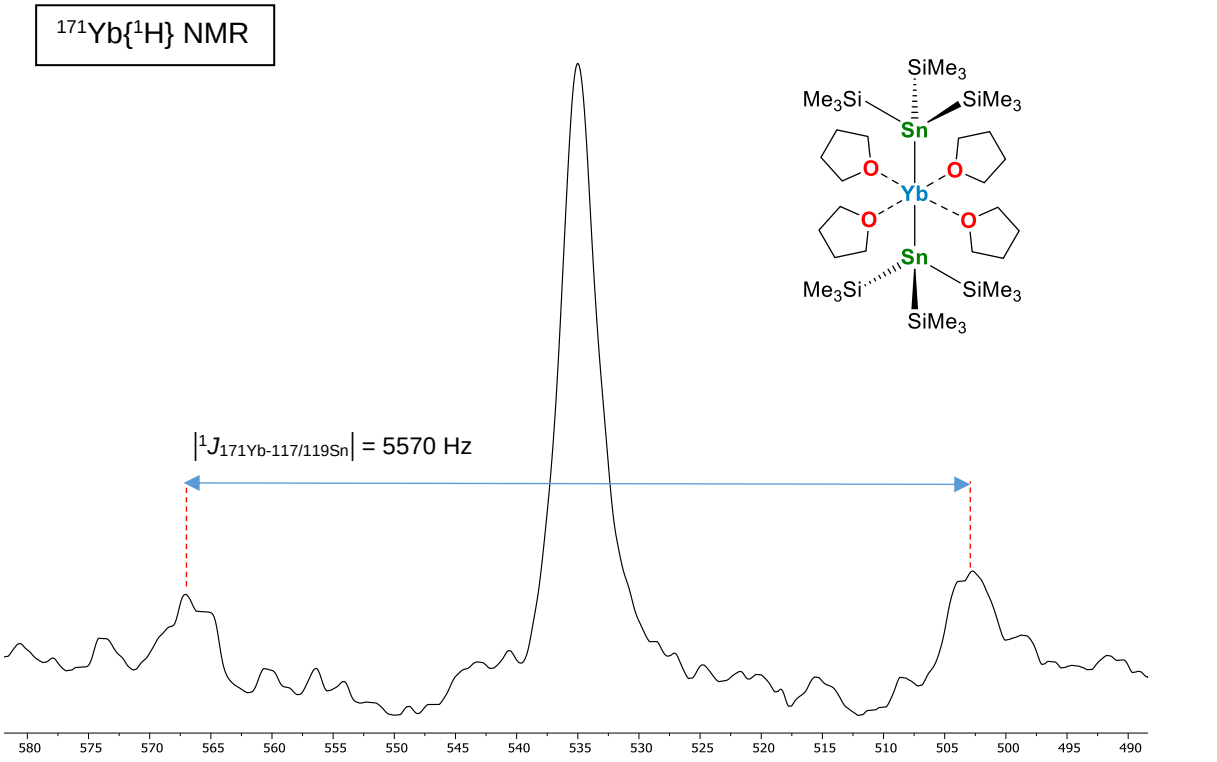

Figure 4. ^{171}Yb{^{1}H} NMR spectrum (87.57 MHz, benzene-d_6, 300 K) of [Yb{Sn(SiMe$_3$)$_3$}$_2$.(thf)$_4$] (**Yb-Sn**).

XRD analysis of the distannyl **Yb-Sn** reveals a very slightly distorted six-coordinate octahedral geometry around the Yb(II) atom with the two $\{Sn(SiMe_3)_3\}^-$ ligands at the axial positions (Figure 5). The Yb-Sn interatomic distances (3.3285(4) and 3.3308(4) Å) are slightly longer than in the isostructural **Ca-Sn** (3.3164(3) Å), and within the range of the other previously reported Yb-Sn complexes: the four-coordinate $[Yb\{Sn(CH_2{}^tBu)_3\}_2.(thf)_2]$ (3.216(1) Å),[21] the octahedral $[Yb\{Sn(SnMe_3)_3\}_2.(thf)_4]$ (3.289(5)-3.300(4) Å)[23] and $[Yb(SnPh_3)_2.(thf)_4]$ (3.305(1) Å),[22] and the trimetallic $[(thf)_2.(Ph_3Sn)Yb(\mu\text{-}Ph)_3Yb.(thf)_3]$ (3.379(1) Å).[24] The Yb-O bond distances (2.420(3)-2.440(3) Å) are slightly longer than in $[Yb\{SnPh_3\}_2.(thf)_4]$ (2.378(21)-2.384(19) Å), though are similar to those in $[Yb\{Sn(SnMe_3)_3\}_2.(thf)_4]$ (2.40(1)-2.41(1) Å). They are also longer than in the calcium derivative **Ca-Sn** (2.353(2)-2.392(3) Å). Compound **Yb-Sn** displays an almost linear Sn-Yb-Sn bond angle (178.452(10)°), very similar to the quasi-linear **Ca-Sn** (178.29(2)°). The Si_i-Sn-Si_j angles around Sn1 (97.47(5)-100.01(5)°) and Sn2 (95.92(5)-102.39(5)°) in **Yb-Sn** span over a greater range than in the calcium congener (96.93(3)-100.58(3)°). They are close to 90°, highlighting the absence of hybridisation between the 5*s* and 5*p* orbitals at tin, and hence point at both an essentially *s*-character, non-directional lone pair of electrons, with highly polarised $^{\delta-}$Sn-Yb$^{\delta+}$ bonds. As expected for the octahedral geometry about the central ytterbium, the Sn_i-Yb-O_j angles are all close to 90° (87.07(8)-91.48(8)°).

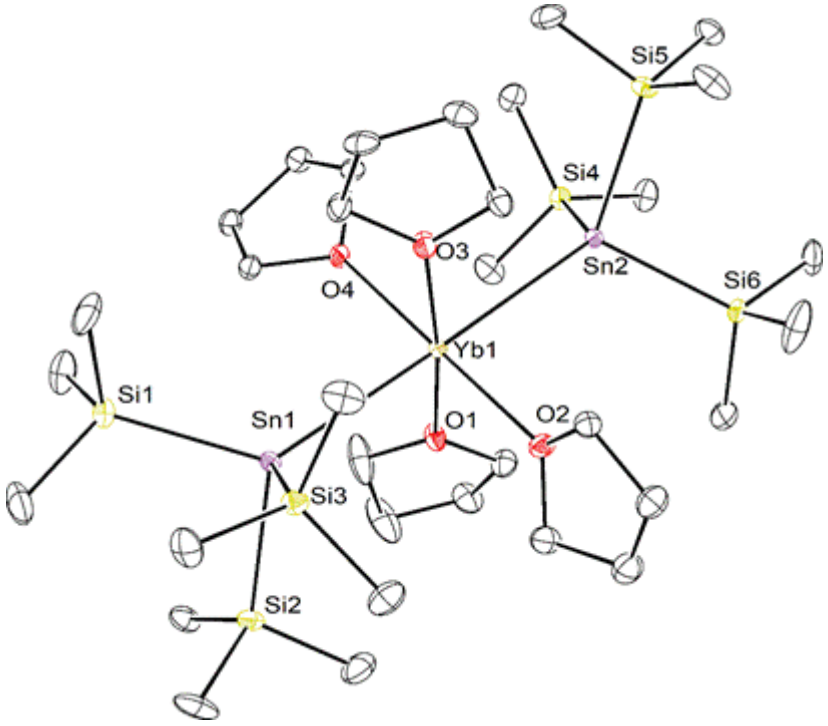

Figure 5. ORTEP representation of $[Yb\{Sn(SiMe_3)_3\}_2\}.(thf)_4]$ (**Yb-Sn**). Ellipsoids at the 30% probability level. Only the major component of the disordered thf molecules shown. Hydrogen atoms omitted for clarity. Selected bond distances (Å) and angles (°): Yb1-Sn1 = 3.3308(4), Yb1-Sn2 = 3.3285(4), Yb1-O1 = 2.440(3), Yb1-O2 = 2.437(3), Yb1-O3 = 2.425(3), Yb1-O4 = 2.420(3), Sn1-Si1 = 2.6009(15), Sn1-Si2 = 2.5923(14), Sn1-Si3 = 2.5968(14), Sn2-Si4 = 2.6048(14), Sn2-Si5 = 2.5929(14), Sn2-Si6 = 2.5885(14); Sn1-Yb1-Sn2 = 178.452(10), O1-Yb1-O2 = 92.23(12), O1-Yb1-O3 = 173.26(11), O1-Yb1-O4 = 88.52(12), O2-Yb1-O3 = 94.27(12), O2-Yb1-

O4 = 179.23(12), O3-Yb1-O4 = 84.99(12), O1-Yb1-Sn1 = 98.18(8), O1-Yb1-Sn2 = 90.19(8), O2-Yb1-Sn1 = 89.67(9), O2-Yb1-Sn2 = 90.99(9), O3-Yb1-Sn1 = 87.07(8), O3-Yb1-Sn2 = 91.48(8), O4-Yb1-Sn1 = 90.48(8), O4-Yb1-Sn2 = 88.84(8), Si1-Sn1-Si2 = 100.01(5), Si1-Sn1-Si3 = 97.47(5), Si2- Sn1-Si3 = 97.90(5), Si4-Sn2-Si5 = 95.92(5), Si4-Sn2-Si6 = 102.39(5), Si5-Sn2-Si6 = 99.60(5).

The germyl **Yb-Ge** forms a five-coordinate distorted square pyramidal geometry ($\tau_5 = 0.46$), with two thf ligands (corresponding to O1 and O2; O1-Yb1-O2 = 152.75(16)°) occupying the apical positions (Figure 6). The four atoms Yb1, Ge1, Ge2 and O3 are nearly coplanar, and the Ge1-Yb1-Ge2, O3-Yb-Ge1 and O3-Yb1-Ge2 angles (125.048(17), 112.20(9) and 122.73(10)°) are relatively close to 120°. The Yb-Ge bond lengths (3.0738(6) and 3.0356(6) Å) in **Yb-Ge** are shorter than those for other Yb(II)-Ge bonds, such as in the six-coordinate compounds [$Yb(GePh_3)_2.(thf)_4$] (3.141(2) and 3.170(2) Å)[25] and [*cyclo*-$(Ph_2Ge)_4Yb.(thf)_4$] (3.104(2) Å),[26] as expected for a complex with a lower coordination number. The Yb-O bond lengths in **Yb-Ge** (2.404(4)-2.440(4) Å) are comparable to those for the known Yb(II)-Ge compounds (2.402(2)-2.475(8) Å) and in **Yb-Sn**. The Si_i-Sn-Si_j angles around Ge1 (99.93(7)-104.70(6)°) and Ge2 (100.57(7)-101.51(6)°) in **Yb-Ge** are larger than the corresponding ones around the tin atoms in **Yb-Sn**. This observation reflects the greater ability of the *p* orbitals around the Ge atom to involve in the formation of hybrid orbitals compared to the tin atoms in **Yb-Sn**, due to the lower energy gap between *s* and *p* orbitals in the case of germanium. Finally, the structure of **Yb-Ge** resembles very closely that of its calcium analogue, the five-coordinate [$Ca\{Sn(SiMe_3)_3\}_2\}.(thf)_3$] (**Ca-Ge**).[35] The key interatomic distances in this calcium digermyl, Ca-Ge (3.022(2)-3.067(2) Å), Ca-O (2.364(7)-2.385(7) Å) and Ge-Si (average 2.388 Å).

For comparative purposes, a summary of the main metric parameters for the new complexes **Yb-Ge** and **Yb-Sn**, as well as those for the already reported ytterbium disilyl [$Yb\{Si(SiMe_3)_3\}_2\}.(thf)_3$] (**Yb-Si**)[28] and for their calcium analogues [$Ca\{Si(SiMe_3)_3\}_2\}.(thf)_3$] (**Ca-Si**),[36] [$Ca\{Ge(SiMe_3)_3\}_2\}.(thf)_3$] (**Ca-Ge**)[35] and [$Ca\{Sn(SiMe_3)_3\}_2\}.(thf)_3$] (**Ca-Sn**),[18] is provided in Table 2. For a given tetrel element (E = Si/Ge/Sn), there is remarkably little difference across the Yb(II) and Ca series. The main variation consists in the slightly shorter Ca-O_{thf} interatomic distances compared to the Yb-O_{thf} ones. It results, in part, from the smaller size calcium (r_{ionic}: Ca^{2+}: 1.00 Å; Yb^{2+}: 1.02 Å), although the difference in the respective ionic radii is too small to account for the observed contraction. The geometry about the tetrel element is hardly affected by the nature of the central metal it is bound to. For a given metal (Met = Ca/Yb(II)), the Met-Sn interatomic distance is much greater than the other Met-E bonds for E = Si or Ge, consistently with the much larger size on tin. However, it is interesting to note that the Yb-Ge (resp. the Ca-Ge) interatomic distance is *not* longer than the Yb-Si (resp. the Ca-Si) one, despite the greater covalent radius of germanium compared to silicon (1.20 vs 1.11 Å). The Yb-O_{thf} and Ca-O_{thf} bond lengths for the six-coordinate complexes **Yb-Sn** and **Ca-Sn** are not longer than those in the five-coordinate complexes **Yb-Si**/**Yb-Ge** and **Ca-Si**/**Ca-Ge**. This is probably the outcome of the release of steric pressure within the distannyls due to the greater size of tin. It may also be the expression of a more

ionic Met-E bond, however note that the tabulated electronegativity of tetrel elements do not vary linearly upon ascending group 14 (Pauling electronegativity: Pb, 2.33; Sn, 1.96; Ge, 2.01; Si, 1.9; C, 2.55).

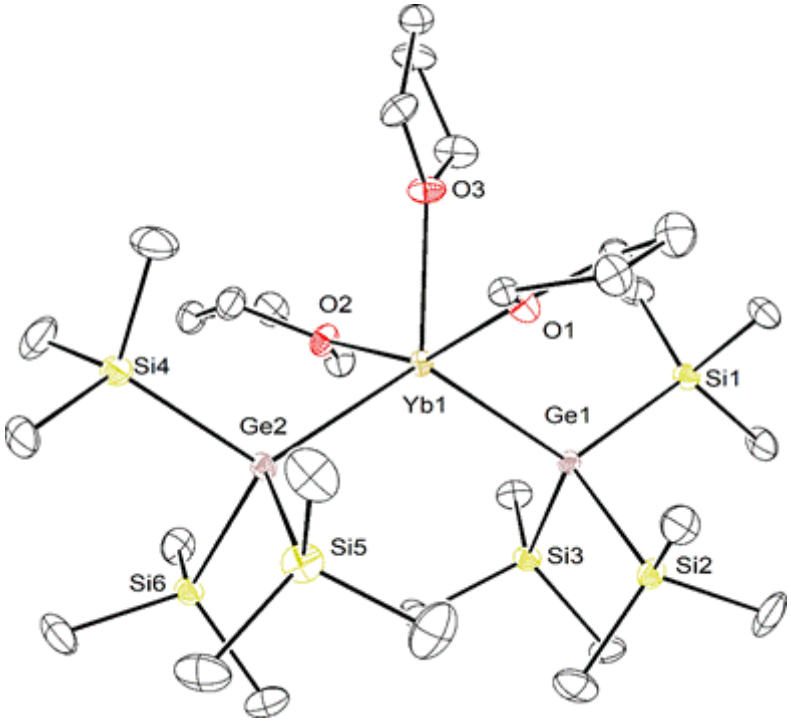

Figure 6. ORTEP representation of [Yb{Ge(SiMe$_3$)$_3$}$_2$}.(thf)$_3$] (**Yb-Ge**). Ellipsoids at the 30% probability level. Only the major component of the disordered thf molecules shown. Hydrogen atoms omitted for clarity. Selected bond distances (Å) and angles (°): Yb1-Ge1 = 3.0356(6), Yb1-Ge2 = 3.0738(6), Yb1-O1 = 2.409(4), Yb1-O2 = 2.404(4), Yb1-O3 = 2.440(4), Ge1-Si1 = 2.3863(16), Ge1-Si2 = 2.3801(18), Ge1-Si3 = 2.3874(16), Ge2-Si4 = 2.3905(17), Ge2-Si5 = 2.3862(19), Ge2-Si6 = 2.3885(16); Ge1-Yb1-Ge2 = 125.048(17), O1-Yb1-O2 = 152.75(16), O1-Yb1-O3 = 75.94(16), O2-Yb1-O3 = 77.05(15), O1-Yb1-Ge1 = 100.03(11), O1-Yb1-Ge2 = 94.70(10), O2-Yb1-Ge1 = 93.41(9), O2-Yb1-Ge2 = 96.80(10), O3-Yb1-Ge1 = 112.20(9), O3-Yb1-Ge2 = 122.73(10), Si1-Ge1-Si2 = 104.70(6), Si1-Ge1-Si3 = 100.75(5), Si2-Ge1-Si3 = 99.93(7), Si4-Ge2-Si5 = 100.57(7), Si4-Ge2-Si6 = 101.51(6), Si5-Ge2-Si6 = 100.79(7).

Table 2. Summary of crystallographic data for complexes [Met{E(SiMe$_3$)$_3$}$_2$}.(thf)$_n$] with Met = Yb/Ca, E = Si/Ge/Sn, and n = 3 or 4.

Compound		Met-E [Å]	Met-O$_{thf}$ [Å]	E-Si [Å] (av.)	E-Met-E [°]	Si-E-Si [°] (av.)	Reference
[Yb{Si(SiMe$_3$)$_3$}$_2$}.(thf)$_3$]	**Yb-Si**	3.0644(6)	2.4210(13)-2.435(2)	2.348	124.51(2)	102.20	28
[Yb{Ge(SiMe$_3$)$_3$}$_2$}.(thf)$_3$]	**Yb-Ge**	3.0356(6)-3.0738(6)	2.404(4)-2.440(4)	2.3865	125.048(17)	101.37	this work
[Yb{Sn(SiMe$_3$)$_3$}$_2$}.(thf)$_4$]	**Yb-Sn**	3.3285(4)-3.3308(4)	2.420(3)-2.440(3)	2.5960	178.452(10)	98.81	this work
[Ca{Si(SiMe$_3$)$_3$}$_2$}.(thf)$_3$]	**Ca-Si**	3.0421(19)-3.0861(19)	2.348(2)-2.389(2)	2.344	125.53(3)	101.75	36
[Ca{Ge(SiMe$_3$)$_3$}$_2$}.(thf)$_3$]	**Ca-Ge**	3.0223(2)-3.0670(2)	2.364(7)-2.385(7)	2.388	125.43(6)	101.16	35
[Ca{Sn(SiMe$_3$)$_3$}$_2$}.(thf)$_4$]	**Ca-Sn**	3.3649(7)-3.3653(7)	2.353(2)-2.392(3)	2.6037	178.29(2)	98.47	18

Bonding analysis

The electronic structure of the complexes discussed above was investigated by the means of Density Functional theory (DFT) calculations at the TZP/PBE0-D3-ZORA level (see Computational Details). All the geometries were fully optimised (gas-phase considered), starting from their structures established by X-ray diffraction analysis when available, or otherwise from that of their closest parent. We first discuss the six-coordinate series of *tetrasolvated* complexes [Yb{E($SiMe_3$)$_2$.(thf)$_4$] (E = Si, Ge, Sn), of which only the Sn derivative (**Yb-Sn**) has been so far isolated (see above; only 3 thf molecules are found in **Yb-Si** and **Yb-Ge**). The calcium relative [Ca{Sn($SiMe_3$)$_2$.(thf)$_4$] (**Ca-Sn**)[18] is added for comparison. Selected computed data are provided in Tables 3-5. The optimised geometries of **Yb-Sn** and **Ca-Sn** are in an overall good agreement with their X-ray structures, with, however, shorter Met-Sn distances. Such underestimation of this specific type of bonds has been observed previously, and is a tendency intrinsic to the method of calculations that is already documented.[18,24]

Within the set of tetrasolvated Yb complexes, the HOMO-LUMO gap decreases when descending group 14 from Si to Sn, whereas the increase of the Wiberg bond indices (WBI) and the variation of the Yb NAO charges are consistent with an increase in Yb-E covalency (Table 3). This apparent contradiction between the variations of the HOMO-LUMO gap and covalency is rationalised by the fact that the frontier orbitals of the complexes are not associated with Yb-ligand bonding. The HOMOs are the seven (non-bonding) 4*f* orbitals and the LUMOs are better seen as describing diffuse Rydberg states loosely bounds to the methyl hydrogens. The two orbitals associated with the Yb-E bonding electron pairs are located below the seven nearly-degenerated 4*f* HOMOs. They can be viewed as the out-of-phase and in-phase combinations of localised Yb-E σ-bonding orbitals, respectively (see Figure 7 for the illustrative example of **Yb-Sn**). They are largely E-polarised, with, from Si to Ge and Sn, E(%)/Yb(%) composition of 84/15, 82/15 and 67/27 for the HOMO-7 and 92/3, 82/14 and 81/13 for the HOMO-8, respectively. These values are indicative of the strong ionic character of Yb-E bonding. The (weak) covalency which increases when descending the tetrel column can be related to a stronger interaction of the valence n*p* AO of E with the 6*s* AO of Yb.

Comparison of the computed data in Table 3 for [Yb{Sn($SiMe_3$)$_3$}$_2$.(thf)$_4$] (**Yb-Sn**) with those of [Ca{Sn($SiMe_3$)$_3$}$_2$.(thf)$_4$] (**Ca-Sn**) shows that the Ca-Sn bond is tangibly more ionic than its Yb-Sn congener. The larger covalency of the Yb-Sn bond is not related to the 4*f*(Yb) orbitals, which remain as expected fully non-bonding, but rather to the comparatively greater participation to the bonding of its 5*d* AOs, as compared to the 3*d*(Ca) orbitals, compare the NAO 5*d* and 3*d* populations of 0.43 and 0.08, respectively.

Another point-of-view on the nature of the Met-E bonding in the [Met{E($SiMe_3$)$_2$.(thf)$_4$] series displayed in Table 3 can be obtained by performing an energy decomposition analysis (EDA) of the interaction between two frozen molecular fragments, according to the Morokuma-Ziegler procedure.[37-39] The decomposition of the total bonding energy (TBE) between the "solvated" cation [Met(thf)$_4$]$^{2+}$ and the [($SiMe_3$)E...E($SiMe_3$)]$^{2-}$ dimeric fragment in the complexes is provided in Table 4.

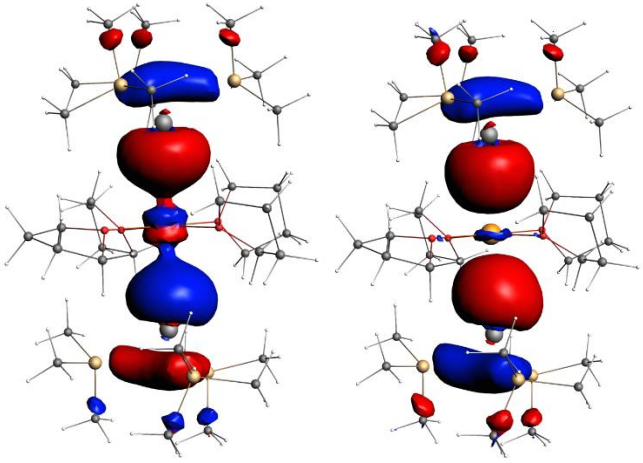

HOMO-7 **HOMO-8**

Figure 7. The two occupied Kohn-Sham orbitals associated with the Yb-Sn bonds in the ytterbium distannylide [Yb{Sn(SiMe$_3$)$_2$.(thf)$_4$] (**Yb-Sn**).

TBE is expressed as the sum of four components: the Pauli repulsion (E_{Pauli}), the electrostatic interaction energy (E_{elstat}), the orbital interaction energy (E_{orb}) and the component associated with the dispersion forces (E_{disp}). The four compounds have similar TBEs. Their moderate variation indicates that the Yb-E bond strength increases in the order Sn < Si < Ge. The Ca-to-Sn bond in **Ca-Sn** is weaker than that of **Yb-Sn**. In any case, these variations are rather weak. For all the computed compounds, TBE is dominated by its electrostatic component, indicating a prevailing ionic bonding. The E_{orb} component, which is associated with covalency, is about 4 times smaller, and the observed trend for E_{orb} within the suite is not fully consistent with that of the Met-E WBI values given in Table 3. Such apparent contradiction with the monotonous variation of the WBIs within the series is not uncommon[18] when the differences between values are small, as in the present scenario. It can be, *inter alia*, related to the arbitrary choice of fragmentation upon which our EDA analysis is built.[40] It should be however mentioned that the alternative chemically intuitive fragmentation [Yb{E(SiMe$_3$)$_3$}(thf)$_4$]$^+$ + [E(SiMe$_3$)$_3$]$^-$ provides similar trends across the investigated series.

A different angle on the Met-E bonding analysis can also be provided by the Quantum Theory of Atoms in Molecules (QTAIM) approach.[41-42] Selected QTAIM data are collated in Table 5. The AIM atomic charges, delocalisation index and electron densities at the bond critical points indicate similar trends as the NAO charges and WBI indices, that is, a gradual (and relative) increase of the covalent nature of the Met-E bond following the order Ca-Sn < Yb-Si < Yb-Ge < Yb-Sn. It is also of note that all the Met-E bond critical point (bcp) indicators have small absolute values. The positive sign of the Laplacian density, the negative sign of the (very small) energy density and the $|V|/G$ ratio significantly larger than 1 are indicative of a bonding mode dominated by an ionic interaction with some very polar covalent character.

For comparison, selected computed data for the Yb trisolvated series [Yb{E(SiMe$_3$)$_3$}$_2$.(thf)$_3$] (E = Si, **Yb-Si**; Ge, **Yb-Ge**; Sn, not isolated) are provided in Tables 6-8. The optimised geometries of the experimentally isolated **Yb-Si** and **Yb-Si** complexes are in good agreement with their X-ray structures. The data collected in Table 6 indicate a significant Yb-E covalent character in the case of E = Sn, due to a stronger interaction between the orbitals 6*s*(Yb) and 5*p*(Sn). The EDA analysis based on a fragmentation between the "solvated" cation $[Yb(thf)_3]^{2+}$ and the $[(SiMe_3)E...E(SiMe_3)]^{2-}$ dimeric fragment (Table 7) and the QTAIM analysis (Table 8) overall provide similar tendencies. Unsurprisingly, the Yb-E bonding is found to be stronger in the case of the trisolvated complexes with respect to their tetrasolvated analogues, both in terms of covalency and ionicity.

Finally, the question of the isolation of **Yb-Sn** as a tetrasolvated species, whereas the related **Yb-Ge** (this work) and **Yb-Si**[28] complexes were obtained as trisolvated species, has been explored. Part of the answer is provided by the computed energy differences $\Delta E = E$[Yb{E(SiMe$_3$)$_3$}$_2$.(thf)$_4$] – E[Yb{E(SiMe$_3$)$_3$}$_2$.(thf)$_3$] – E(thf). The three values are negative (–15.4, –15.9 and –21.7 kcal/mol for E = Si, Ge and Sn, respectively), indicating that for the whole suite, tetrasolvated species are more stable in vacuum. In solution in thf, explicit solvent effect should be considered,[43] which would require a computational effort that is far beyond the scope of this investigation. It can however be noted that the value of ΔE corresponding to E = Sn is far more negative than for its Si and Ge congeners, highlighting the enhanced stability of the tetrasolvated species with respect to the trisolvated one in the specific case of Sn. Energy decomposition analysis indicates that with Sn, the major contribution responsible for the lower value of ΔE is the Pauli repulsion, which can be in that particular case approximated to steric repulsion. It thus appears that in the investigated ytterbium ditetryl complexes, tin offers greater flexibility and room around the central ytterbium than silicon and germanium do, with the consequence that the hosting of a fourth thf molecule in the coordination sphere of ytterbium becomes favourable. This is consistent with accepted wisdom, since the sterically shielding Ph groups on the tetrel elements will be located further away from ytterbium as the size of the tetrel increases.

Conclusions

We have prepared the ytterbium(II) distannylide [Yb{Sn(SiMe$_3$)$_3$}$_2$.(thf)$_4$] (**Yb-Sn**), which we have fully characterised, including by X-ray diffraction analysis and high-resolution NMR spectroscopy in benzene-d_6. The octahedral tetrasolvated complex, with stannyl groups in axial position, exhibits in particular well-defined resonances at $\delta_{^{119}Sn}$ –757 ppm and $\delta_{^{171}Yb}$ 5570 ppm in the ^{119}Sn and ^{171}Yb NMR spectra, respectively. It is a rare case where both XRD and multinuclear NMR data have been collated for an Yb(II) stannylide, and it adds to the limited set of such complexes documented in the literature. The NMR and structural data for the stannylide **Yb-Sn** have been compared to those obtained for its derivatives incorporating lighter tetrels, namely, the known[28] five-coordinate [Yb{Si(SiMe$_3$)$_3$}$_2$.(thf)$_3$] (**Yb-Si**) and the new [Yb{Ge(SiMe$_3$)$_3$}$_2$.(thf)$_3$] (**Yb-Ge**), which have also been comprehensively

characterised. Variations in the chemical shifts and coupling constants are detectable across the complexes, and they can be tentatively linked to the variation of coordination numbers and bonding in these complexes.

DFT calculations, completed with NBO, EDA and QTAIM analyses, have shed light on the nature of the metal-to-tetrel bond in these three ytterbium complexes and in the related calcium distannylide [Ca{Sn(SiMe$_3$)$_3$}$_2$.(thf)$_4$] (**Ca-Sn**). In all computed compounds, the metal-to-tetrel bonding is found to be of prevailing ionic character, with only a weak covalent component. This is likely the reason why no relationship could be found between the NMR coupling constants and the degree of covalency in these compounds. Nevertheless, this weak covalency is stronger in the case of the heavier tetrel element considered, tin. It is also found to be more important in **Yb-Sn** than in **Ca-Sn**, due to the availability of the 5*d*(Yb) orbitals for bonding.

Table 3. Relevant DFT-computed data for the six-coordinate complexes [Met{E(SiMe$_3$)$_3$}$_2$.(thf)$_4$] (Met = Yb, E = Si, Ge, Sn; Met = Ca, E = Sn).

		[Yb{Si(SiMe$_3$)$_3$}$_2$.(thf)$_4$] (putative)	[Yb{Ge(SiMe$_3$)$_3$}$_2$.(thf)$_4$] (putative)	[Yb{Sn(SiMe$_3$)$_3$}$_2$.(thf)$_4$] (**Yb-Sn**)	[Ca{Sn(SiMe$_3$)$_3$}$_2$.(thf)$_4$] (**Ca-Sn**)
HOMO-LUMO gap / eV		4.20	4.17	4.00	4.60
Met-E /Å[a] [WBI][a,b]		3.224 [0.207]	3.160 [0.209]	3.250 [0.270]	3.251 [0.159]
Met-O$_{thf.}$/Å[a] [WBI][a,b]		2.439 [0.037]	2.436 [0.039]	2.434 [0.045]	2.386 [0.032]
∠ E-Met-E'/ °		174	176	175	176
NAO charges and configurations	Met	1.38 ($4f^{13.98}$ $5d^{0.41}$ $6s^{0.17}$ $6p^{0.01}$)	1.38 ($4f^{13.98}$ $5d^{0.42}$ $6s^{0.17}$ $6p^{0.01}$)	1.33 ($4f^{13.98}$ $5d^{0.43}$ $6s^{0.22}$ $6p^{0.01}$)	1.71 ($4s^{0.21}$ $4p^{0.01}3d^{0.08}$)
	E[a]	–0.86 (**3**$s^{1.43}$ $3p^{3.40}$)	–0.90 (**4**$s^{1.50}$ $4p^{3.38}$)	–0.70 (**5**$s^{1.51}$ $5p^{3.16}$)	–0.75 (**5**$s^{1.56}$ $5p^{3.18}$)
	O[a]	–0.62	–0.60	–0.61	–0.61

[a] Averaged values. [b] WBI = Wiberg bond index given in brackets.

Table 4. Morokuma-Ziegler energy decomposition analysis in the six-coordinate complexes [Met{E(SiMe$_3$)$_3$}$_2$.(thf)$_4$] (Met = Yb, E = Si, Ge, Sn; Met = Ca, E = Sn).[a]

Fragmentation	[Met(thf)$_4$]$^{2+}$ + [{E(SiMe$_3$)$_3$}$_2$]$^{2-}$			
	[Yb{Si(SiMe$_3$)$_3$}$_2$.(thf)$_4$] (putative)	[Yb{Ge(SiMe$_3$)$_3$}$_2$.(thf)$_4$] (putative)	[Yb{Sn(SiMe$_3$)$_3$}$_2$.(thf)$_4$] (**Yb-Sn**)	[Ca{Sn(SiMe$_3$)$_3$}$_2$.(thf)$_4$] (**Ca-Sn**)
E_{Pauli}	*4.09*	*4.34*	*4.48*	*3.83*
E_{elstat}	*–13.47*	*–13.60*	*–13.74*	*–13.04*
E_{orb}	*–3.52*	*–3.68*	*–3.66*	*–3.54*
E_{disp}	*–1.47*	*–1.50*	*–1.40*	*–1.38*
TBE[b]	–14.37	–14.44	–14.32	–14.13

[a] All values in eV. [b] Total bonding energy (TBE) = $E_{\text{Pauli}} + E_{\text{elstat}} + E_{\text{orb}} + E_{\text{disp}}$.

Table 5. QTAIM descriptors of the Met-E bonds in the six-coordinate complexes [Met{$E(SiMe_3)_3$}$_2$.$(thf)_4$] (Met = Yb, E = Si, Ge, Sn; Met = Ca, E = Sn).[a,b]

		[Yb{$Si(SiMe_3)_3$}$_2$.$(thf)_4$] (putative)	[Yb{$Ge(SiMe_3)_3$}$_2$.$(thf)_4$] (putative)	[Yb{$Sn(SiMe_3)_3$}$_2$.$(thf)_4$] (**Yb-Sn**)	[Ca{$Sn(SiMe_3)_3$}$_2$.$(thf)_4$] (**Ca-Sn**)
Atom charges	Met	1.54	1.53	1.51	1.57
	E[a]	–0.21	–0.62	–0.30	–0.32
	O[a]	–1.06	–1.06	–1.05	–1.06
Delocalisation index	δ[a]	0.245	0.255	0.275	0.197
bcp indicators[a]	ρ	0.023	0.024	0.025	0.021
	$\nabla^2\rho$	+0.031	+0.035	+0.032	+0.030
	H	–0.003	–0.003	–0.004	–0.002
	V	–0.013	–0.014	–0.015	–0.012
	$\lvert V \rvert$/G	1.26	1.25	1.31	1.21

[a] Averaged values. [b] ρ, $\nabla^2\rho$, H, V and G are the electron density, Laplacian of ρ density, energy density, potential energy density and kinetic energy density values at the Met-E bond critical point (bcp), respectively. All values in a.u.

Table 6. Relevant DFT-computed data for the five-coordinate complexes [Yb{E(SiMe$_3$)$_3$}$_2$.(thf)$_3$] (E = Si, Ge, Sn).

		[Yb{Si(SiMe$_3$)$_3$}$_2$.(thf)$_3$] (**Yb-Si**)	[Yb{Ge(SiMe$_3$)$_3$}$_2$.(thf)$_3$] (**Yb-Ge**)	[Yb{Sn(SiMe$_3$)$_3$}$_2$.(thf)$_3$] (putative)
HOMO-LUMO gap / eV		3.92	3.93	3.91
Met-E /Å[a] [WBI][a,b]		2.991 [0.275]	2.977 [0.275]	1.137 [0.345]
Met-O$_{thf.}$/Å[a] [WBI][a,b]		2.194 [0.031]	2.434 [0.042]	2.425 [0.046]
∠ E-Met-E'/ °		126	125	122
NAO charges	Met	1.33 ($4f^{13.97}\,5d^{0.38}\,6s^{0.24}\,6p^{0.00}$)	1.34 ($4f^{13.97}\,5d^{0.39}\,6s^{0.23}\,6p^{0.01}$)	1.29 ($4f^{13.97}\,5d^{0.35}\,6s^{0.31}\,6p^{0.00}$)
	E[a]	–0.90 ($3s^{1.40}\,3p^{3.46}$)	–0.97 ($4s^{1.48}\,4p^{3.45}$)	–0.72 ($5s^{1.50}\,5p^{3.21}$)
	O[a]	–0.62	–0.61	–0.62

[a] Averaged values. [b] WBI = Wiberg bond index.

Table 7. Morokuma-Ziegler energy decomposition analysis in the five-coordinate complexes $[Yb\{E(SiMe_3)_3\}_2.(thf)_3]$ (E = Si, Ge, Sn).[a]

Fragmentation		$[Yb(thf)_3]^{2+} + [\{E(SiMe_3)_3\}_2]^{2-}$	
	$[Yb\{Si(SiMe_3)_3\}_2.(thf)_3]$ (**Yb-Si**)	$[Yb\{Ge(SiMe_3)_3\}_2.(thf)_3]$ (**Yb-Ge**)	$[Yb\{Sn(SiMe_3)_3\}_2.(thf)_3]$ (putative)
E_{Pauli}	*4.53*	*4.40*	*4.65*
E_{elstat}	*–14.97*	*–14.60*	*–14.94*
E_{orb}	*–4.35*	*–4.33*	*–4.49*
E_{disp}	*–0.96*	*–0.87*	*–0.98*
TBE[b]	–15.76	–15.40	–15.76

[a] All values in eV. [b] Total bonding energy (TBE) = $E_{Pauli} + E_{elstat} + E_{orb} + E_{disp}$.

Table 8. QTAIM descriptors of the Yb-E bonds in the five-coordinate complexes $[Yb\{E(SiMe_3)_3\}_2.(thf)_3]$ (E = Si, Ge, Sn).[a,b]

		$[Yb\{Si(SiMe_3)_3\}_2.(thf)_3]$ (**Yb-Si**)	$[Yb\{Ge(SiMe_3)_3\}_2.(thf)_3]$ (**Yb-Ge**)	$[Yb\{Sn(SiMe_3)_3\}_2.(thf)_3]$ (putative)
Atom charges	Met	1.46	1.45	1.42
	E[a]	–0.29	–0.70	–0.36
	O[a]	–1.06	–1.04	–1.06
Delocalisation index	δ[a]	0.369	0.366	0.372
bcp indicators[a]	ρ	0.033	0.033	0.030
	$\nabla^2\rho$	+0.041	+0.047	+0.036
	H	–0.006	–0.006	–0.005
	V	–0.023	–0.023	–0.020
	$\lvert V \rvert /G$	1.374	1.332	1.364

[a] Averaged values. [b] ρ, $\nabla^2\rho$, H, V and G are the electron density, Laplacian of ρ density, energy density, potential energy density and kinetic energy density values at the Met-E bond critical point (bcp), respectively. All values in a.u.

Experimental section

General considerations

All manipulations were performed under an inert atmosphere by using standard Schlenk techniques or in a dry, solvent-free glovebox (Jacomex; O_2<1 ppm, H_2O<3 ppm). Hexanes (petroleum ether), toluene, dichloromethane, and Et_2O were collected from MBraun SPS-800 purification alumina columns and thoroughly degassed with argon before being stored on 4 Å molecular sieves; thf was distilled under argon from Na/benzophenone prior to use. Deuterated solvents (Eurisotop, Saclay, France) were stored in sealed ampoules over activated 4 Å molecular sieves and degassed by a minimum of three freeze–thaw cycles. Standard NMR spectra (see below for high-resolution data) were recorded with Bruker AM-400 or AM-500 spectrometers. All ^{1}H and ^{13}C chemical shifts (δ, reported in ppm) were determined relative to the residual signal of the deuterated solvent. Assignment of the signals was assisted by 1D (^{1}H, ^{13}C) NMR experiments. [K(Si(SiMe$_3$)$_3$)],[44] [Ge(SiMe$_3$)$_4$],[45] [Sn(SiMe$_3$)$_4$],[46-47] YbI$_2$.(thf)$_2$[48] and [Yb{Si(SiMe$_3$)$_3$}.(thf)$_3$][28] were prepared following literature procedures. All other chemicals were provided by commercial suppliers and used as received. Satisfactory combustion analysis of the complexes could not be achieved, likely due to their extreme air- and moisture-sensitivity.

Synthesis of [Yb{Sn(SiMe$_3$)$_3$}$_2$}.(thf)$_4$] (Yb-Sn). To a Schlenk flask was added Sn(SiMe$_3$)$_4$ (500 mg, 1.22 mmol) and KO^{t}Bu (137 mg, 1.22 mmol), and the contents were dissolved in thf (7 mL). The pale-yellow solution was left to stir for 1 h, before it was added dropwise to a suspension of YbI$_2$.(thf)$_2$ (240 mg, 0.82 mmol) in thf (15 mL) at room temperature. The suspension was left to stir overnight. The thf was removed under reduced pressure and the residue extracted into hexanes (30 mL). The solution was isolated via cannula filtration, concentrated to 5 mL and transferred to a −30 °C freezer to give the compound as pale yellow crystals, which were isolated by filtration. Further concentration of the mother liquor gave a second crop of crystals suitable for an X-ray diffraction study. Yield: 252 mg (41%)

^{1}H NMR (500.13 MHz, benzene-d_6, 300 K): δ 3.80 (m, 16H, 2,5-C*H*$_2$-thf), 1.47 (m, 16H, 3,4-C*H*$_2$-thf), 0.57 (br s, 54H, SiC*H*$_3$) ppm.

^{13}C{^{1}H} NMR (100.65 MHz, benzene-d_6, 300 K): δ 68.60 (2,5-*C*H$_2$-thf), 25.22 (3,4-*C*H$_2$-thf), 6.75 ($|^{1}J_{^{13}C\text{-}^{29}Si}|$ = 37.5 Hz, $|^{2}J_{^{13}C\text{-}^{117/119}Sn}|$ = 6.7 Hz, Si*C*H$_3$) ppm.

^{29}Si{^{1}H} NMR (99.36 MHz, benzene-d_6, 300 K): δ −10.9 ($|^{1}J_{^{29}Si\text{-}^{119}Sn}|$ = 66.2 Hz, $|^{1}J_{^{29}Si\text{-}^{117}Sn}|$ = 63.1 Hz, $|^{1}J_{^{29}Si\text{-}^{13}C}|$ = 37.5 Hz, $|^{2}J_{^{29}Si\text{-}^{171}Yb}|$ = 30.5 Hz, $|^{3}J_{^{29}Si\text{-}^{117/119}Sn}|$ = 5.4 Hz) ppm.

^{119}Sn{^{1}H} NMR (186.36 MHz, benzene-d_6, 300 K): δ –757 ($|^{1}J_{^{119}Sn\text{-}^{171}Yb}|$ = 5570 Hz, $|^{2}J_{^{119}Sn\text{-}^{117}Sn}|$ = 932 Hz) ppm.

^{171}Yb NMR (87.57 MHz, benzene-d_6, 300 K): δ 535 ($|^{1}J_{^{171}Yb\text{-}^{119}Sn}|$ = 5570 Hz) ppm.

Synthesis of [Yb{Ge(SiMe$_3$)$_3$}$_2$}.(thf)$_3$] (Yb-Ge). To a Schlenk flask was added Ge(SiMe$_3$)$_4$ (390 mg, 1.07 mmol) and KO^{t}Bu (120 mg, 1.07 mmol), and the contents were dissolved in thf (15 mL). The pale-yellow solution was left to stir for 1 h, before it was added dropwise to a suspension of YbI$_2$.(thf)$_2$ (300

mg, 0.53 mmol) in thf (15 mL) at room temperature. The suspension was left to stir overnight. The thf was removed under reduced pressure and the residue was extracted into hexanes (30 mL). The solution was isolated via cannula filtration, concentrated to 5 mL and transferred to a −30 °C freezer to give the compound as slightly dark yellow/orange crystals, which were isolated by filtration and dried under reduced pressure. Further concentration of the mother liquor gave a second crop of crystals suitable for an X-ray diffraction study. Yield: 254 mg (32%)

^{1}H NMR (500.13 MHz, benzene-d_6, 300 K): δ 3.69 (m, 12H, 2,5-CH_2-thf), 1.40 (m, 12H, 3,4-CH_2-thf), 0.53 (br s, 54H, SiCH_3) ppm.

^{13}C{^{1}H} NMR (125.77 MHz, benzene-d_6, 300 K): δ 68.73 (2,5-CH$_2$-thf), 25.19 (3,4-CH$_2$-thf), 7.32 ($|^{1}J_{^{13}C\text{-}^{29}Si}|$ = 37.5 Hz, $|^{3}J_{^{13}C\text{-}^{171}Yb}|$ = 6.8 Hz, SiCH$_3$) ppm.

^{29}Si{^{1}H} NMR (99.36 MHz, benzene-d_6, 300 K): δ −2.4 ($|^{1}J_{^{29}Si\text{-}^{13}C}|$ = 37.5 Hz, $|^{2}J_{^{29}Si\text{-}^{171}Yb}|$ = 20.2 Hz) ppm.

^{171}Yb NMR (87.57 MHz, benzene-d_6, 300 K): δ 816 ppm.

High-resolution 1D NMR for compounds Yb-Sn, Yb-Ge and Yb-Si. NMR experiments were carried out by using Bruker AVIII 500 spectrometers (Bruker, Wissembourg, France) equipped with a 10 A gradient amplifier giving a maximum gradient of 50 G.cm^{-1} and a 5 mm BBFO probe including shielded z-gradients. Measuring frequencies were 500 MHz for ^{1}H, 125 MHz for ^{13}C, 186 MHz for ^{119}Sn and 99 MHz for ^{29}Si. ^{1}H and ^{13}C NMR chemical shifts are reported in ppm using the residual peak of benzene-d_6 (7.16 ppm and 128.0 ppm) as internal standard. ^{29}Si, ^{119}Sn and ^{171}Yb NMR spectra were referenced (δ = 0.0 ppm) to calculated ^{29}Si, ^{119}Sn and ^{171}Yb frequencies in Me_4Si, Me_4Sn and Yb(η-C_5Me_5)$_2$(THF)$_2$ references compounds, respectively.[49]

1D ^{1}H. One-dimensional ^{1}H experiments were acquired with standard Bruker "zg" program. The spectra were acquired with sweep width of 10000 Hz and 59998 data points, using 256 scans and the relaxation delay (D1) was 30 s. Exponential window function (LB=0.3) was applied before Fourier transformation.

1D ^{13}C. One-dimensional ^{13}C NMR spectra were recorded with standard Bruker "zgig" program with broadband proton decoupling in order to remove ^{13}C - ^{1}H coupling. The spectra were acquired with sweep width of 50505 Hz and 202014 data points, using 1340 scans and the relaxation delay (D1) was 30 s. Exponential window function (LB=1.5) was applied before Fourier Transformation.

1D ^{29}Si. One-dimensional ^{29}Si experiment were acquired with standard Bruker "dept45" program with broadband proton decoupling in order to remove ^{29}Si - ^{1}H coupling. The spectra were acquired width sweep with of 3894 and 36012 data points, using 1024 scans and the recycling delay was 5 s. Exponential window function (LB=0.2) was applied before Fourier transformation.

1D ^{119}Sn. One-dimensional ^{119}Sn experiments were acquired with standard Bruker "zgig" program. The spectra were acquired with sweep width of 64935 Hz and 194798 data points, using 3072 scans and the recycling delay was 18 s. Exponential window function (LB=10) was applied before Fourier transformation.

1D ^{171}Yb. One-dimensional ^{171}Yb experiments were acquired with standard Bruker "zgig" program. The spectra were acquired with sweep width of 19840 Hz and 59520 data points, using 16384 scans and the relaxation delay (D1) was 2 s. Exponential window function (LB=100) was applied before Fourier transformation.

DFT computational details

Density functional theory (DFT) calculations were performed using the Amsterdam Density Functional ADF2019 code.[50-51] Scalar relativistic effects were addressed through the Zeroth Order Regular Approximation (ZORA).[52] A triple-zeta basis set augmented with a polarisation function (STO-TZP)[53] was used together with the PBE0 functional[54-56] and Grimme's empirical DFT-D3 (BJDAMP) corrections.[57] for geometry optimisation and analytical vibrational frequency computations. Natural atomic orbital (NAO) populations and Wiberg bond indices were computed with the NBO6.0 program.[58] Interaction energy between fragments were computed according to the Morokuma-Ziegler energy decomposition analysis (EDA) formalism[37-39] implemented in the ADF2019 program. The QTAIM analysis[41] was performed as implemented in the ADF2019 suite.[59-60]

Acknowledgements

P.M.C thank the *Agence Nationale de la Recherche* for the provision of a research grant (ANR-17-CE07-0017-01). The GENCI (*Grand Equipment National de Calcul Intensif*) is acknowledged for HPC resources (Project A0050807367). H.O. and G.H. would like to thank the Region Normandie, Rouen University, CNRS, INSA of Rouen, ERDF and the Labex SynOrg (ANR-11-LABX-0029).

Conflicts of interest

There are no conflicts to declare.

Notes and references

1 *Lanthanides: Chemistry and Use in Organic Synthesis*; Ed. S. Kobayashi, Springer, 1999.

2 P. G. Steel, *J. Chem. Soc., Perkin Trans. 1*, 2001, 2727.

3 W. J. Evans, *J. Organomet. Chem.*, 2002, **652**, 61.

4 A. R. Willauer, A. M. Dabrowska, R. Scopelliti and M. Mazzanti, *Chem. Commun.*, 2020, **56**, 8936.

5 M. Xémard, M. Cordier, E. Louyriac, L. Maron, C. Clavaguéra and G. Nocton, *Dalton Trans.*, 2018, **47**, 9226.

6 L. Yan, H. Liu, J. Wang, Yong Zhang and Qi Shen, *Inorg. Chem.*, 2012, **51**, 4151.

7 K. R. Meihaus, M. E. Fieser, J. F. Corbey, W. J. Evans and J. R. Long, *J. Am. Chem. Soc.*, 2015, **137**, 9855.

8 C. A. P. Goodwin, N. F. Chilton, L. S. Natrajan, M.-E. Boulon, J. W. Ziller, W. J. Evans and D. P. Mills, *Inorg. Chem.*, 2017, **56**, 5959.

9 W. J. Evans and H. Katsumata, *Macromolecules*, 1994, **27**, 2330.

10 S. Harder, *Angew. Chem. Int. Ed.*, 2004, **43**, 2714.

11 F. Buch and S. Harder, *Organometallics*, 2007, **26**, 5132.

12 W. Xie, H. Hu and C. Cui, *Angew. Chem. Int. Ed.*, 2012, **51**, 11141.

13 H. Hu and C. Cui, *Organometallics*, 2012, **31**, 1208.

14 B. Liu, T. Roisnel, L. Maron, J.-F. Carpentier and Y. Sarazin, *Chem. Eur. J.*, 2013, **19**, 3986.

15 B. Liu, T. Roisnel, J.-F. Carpentier and Y. Sarazin, *Chem. Eur. J.*, 2013, **19**, 13445.

16 J. M. Keates and G. A. Lawless, *^{171}Yb NMR spectroscopy*; in *Advanced applications of NMR to organometallic chemistry*; Eds. M. Gielen, R. Willem and B. Wrackmeyer, John Wiley & Sons, Chichester, 1996, pp. 357-370.

17 A. G. Avent, M. A. Edelman, M. F. Lappert and G. A. Lawless, *J. Am. Chem. Soc.*, 1989, **111**, 3423.

18 P. M. Chapple, J. Cartron, G. Hamdoun, S. Kahlal, M. Cordier, H. Oulyadi, J.-F. Carpentier, J.-Y. Saillard and Y. Sarazin, *Chem. Sci.*, 2021, **12**, 7098.

19 P. M. Chapple, S. Kahlal, J. Cartron, T. Roisnel, V. Dorcet, M. Cordier, J.-Y. Saillard, J.-F. Carpentier and Y. Sarazin, *Angew. Chem., Int. Ed.*, 2020, **59**, 9120.

20 P. M. Chapple, M. Cordier, V. Dorcet, T. Roisnel, J.-F. Carpentier and Y. Sarazin, *Dalton Trans.*, 2020, **49**, 11878.

21 F. G. N. Cloke, C. I. Dalby, P. B. Hitchcock, H. Karamallakis and G. A. Lawless, *J. Chem. Soc., Chem. Commun.*, 1991, 779.

22 M. N. Bochkarev, V. V. Khramenkov, Y. F. Rad'kov, L. N. Zakharov and Y. T. Struchkov, *J. Organomet. Chem.*, 1991, **408**, 329.

23 L. N. Bochkarev, O. V. Grachev, N. E. Molosnova, S. F. Zhiltsov, L. N. Zakharov, G. K. Fukin, A. I. Yanovsky and Y. T. Struchkov, *J. Organomet. Chem.*, 1993, **443**, C26.

24 M. N. Bochkarev, V. V. Khramenkov, Y. F. Rad'kov, L. N. Zakharov and Y. T. Struchkov, *J. Organomet. Chem.*, 1991, **421**, 29.

25 L. N. Bochkarev, V. M. Makarov, Y. N. Hrzhanovskaya, L. N. Zakharov, G. K. Fukin, A. I. Yanovsky and Y. T. Struchkov, *J. Organomet. Chem.*, 1994, **467**, C3.

26 L. N. Bochkarev, V. M. Makarov, L. N. Zakharov, G. K. Fukin, A. I. Yanovsky and Y. T. Struchkov, *J. Organomet. Chem.*, 1995, **490**, C39.

27 The CIF file available from the CCDC database, code YEDYEL, does not contain structural data.

28 R. Zitz, J. Hlina, K. Gatterer, C. Marschner, T. Szilvási and J. Baumgartner, *Inorg. Chem.*, 2015, **54**, 7065.

29 M. M. Corradi, A. D. Frankland, P. B. Hitchcock, M. F. Lappert and G. A. Lawless, *Chem. Commun.*, 1996, 2323.

30 M. Niemeyer, *Inorg. Chem.*, 2006, **45**, 9085.

31 C. Eaborn, P. B. Hitchcock, K. Izod and J. D. Smith, *J. Am. Chem. Soc.*, 1994, **116**, 12071.

32 B. L. L. Réant, S. T. Liddle and D. P. Mills, *Chem. Sci.*, 2020, **11**, 10871.
33 R. Fischer, J. Baumgartner, C. Marschner and F. Uhlig, *Inorg. Chim. Acta*, 2005, **358**, 3174.
34 J. Fischer, J. Baumgartner and C. Marschner, *Organometallics*, 2005, **24**, 1263.
35 W. Teng and K. Ruhlandt-Senge, *Organometallics*, 2004, **23**, 952.
36 W. Teng and K. Ruhlandt-Senge, *Organometallics*, 2004, **23**, 2694.
37 K. Morokuma, *J. Chem. Phys.*, 1971, **55**, 1236.
38 T. Ziegler and A. Rauk, *Inorg. Chem.*, 1979, **18**, 1558.
39 F. M. Bickelhaupt and E. J. Baerends, *Rev. Comput. Chem.*; K.B. Lipkowitz and D.B. Boyd, Eds.; Wiley, New York 2000, **15**, 1.
40 L. Bondì, A. L. Garden, P. Jerabek, F. Totti and S. Brooker, *Chem. Eur. J.* 2020, **26**, 13677.
41 R. F. W. Bader, *Atoms in Molecules - A Quantum Theory*; Oxford University Press: Oxford, England, 1990.
42 P. L. A. Popelier, in *The Chemical Bond*, Eds. Frenking, G.; Shaik, S., Wiley-VCH, 2014, **1**, 271.
43 When solvent effect is implicitly considered via the COSMO model, ΔE = –11.3, –11.8 and –17.3 kcal/mol are found for E = Si, Ge and Sn, respectively.
44 C. Marschner, *Eur. J. Inorg. Chem.*, 1998, 221.
45 A. G. Brook, F. Abdesaken and H. Sollradl, *J. Organomet. Chem.*, 1986, **299**, 9.
46 H. Buerger and U. Goetze, *Angew. Chem., Int. Ed.*, 1968, **7**, 212.
47 H. Gilman and C. L. Smith, *J. Am. Chem. Soc.*, 1964, **86**, 1454.
48 P. L. Watson, T. H. Tulip and I. Williams, *Organometallics*, 1990, **9**, 1999.
49 R. K. Harris, E. D. Becker, S. M. Cabral De Menezes, R. Goodfellow, P. Granger, *Pure Appl. Chem.*, 2001, **73**,1795.
50 G. te Velde, F. M. Bickelhaupt, S. J. A. van Gisbergen, C. F. Guerra, E. J. Baerends, J. G. Snijders and T. Ziegler, *J. Comput. Chem.*, 2001, **22**, 931.
51 ADF 2019.3, SCM, Theoretical Chemistry, Vrije Universiteit, Amsterdam, The Netherlands, http://www.scm.com.
52 E. van Lenthe, E. J. Baerends and J. G. Snijders, *J. Chem. Phys.*, 1994, **101**, 9783.
53 E. V. Lenthe and E. J. Baerends, *J. Comput. Chem.*, 2003, **24**, 1142.
54 J. P. Perdew, K. Burke and M. Ernzerhof, *Phys. Rev. Lett.*, 1996, **77**, 3865.
55 J. P. Perdew, K. Burke and M. Ernzerhof, *Phys. Rev. Lett.*, 1997, **78**, 1396.
56 C. Adamo and V. Barone, *J. Chem. Phys.*, 1999, **110**, 6158.
57 S. Grimme, *J. Comput. Chem.*, 2006, **27**, 1787.
58 E. D. Glendening, J. K. Badenhoop, A. E. Reed, J. E. Carpenter, J. A. Bohmann, C. M. Morales and F. Weinhold, NBO 6.0, University of Wisconsin (Madison, WI, 2001, http://nbo6.chem.wisc.edu).
59 J. I. Rodríguez, R. F. W. Bader, P. W. Ayers, C. Michel, A. W. Götz and C. Bo, *Chem. Phys. Lett.*, 2009, **472**, 149.

60 J. I. Rodriguez, *J. Comput. Chem.*, 2013, **34**, 681.